Electronic Supplementary Material (ESI) for New Journal of Chemistry.

Supplementary material

Influence of the Ni^{II}/Mn^{II} Ratio on the Physical Properties of Heterometallic $Ni_{2x}Mn_{(2-2x)}P_2S_6$ Phases and Potassium Intercalates $K_{0.8}Ni_{2x}Mn_{(1.6-2x)}P_2S_6 \cdot 2H_2O$

Catalina Cortes[1,2], Pablo Fuentealba[1,2*], Jorge Manzur[1], Juliana Pérez[1,2], Carolina Aliaga[2,3], Nathalie Audebrand[4], Hector Aguilar-Bolados[1], Evgenia Spodine[1,2*]

[1]Facultad de Ciencias Químicas y Farmacéuticas, U. de Chile

[2]CEDENNA

[3]Facultad de Química y Biología, Universidad de Santiago de Chile

[4]Univ Rennes, CNRS, ISCR (Institut des Sciences Chimiques de Rennes) – UMR 6226,

F-35000 Rennes, France.

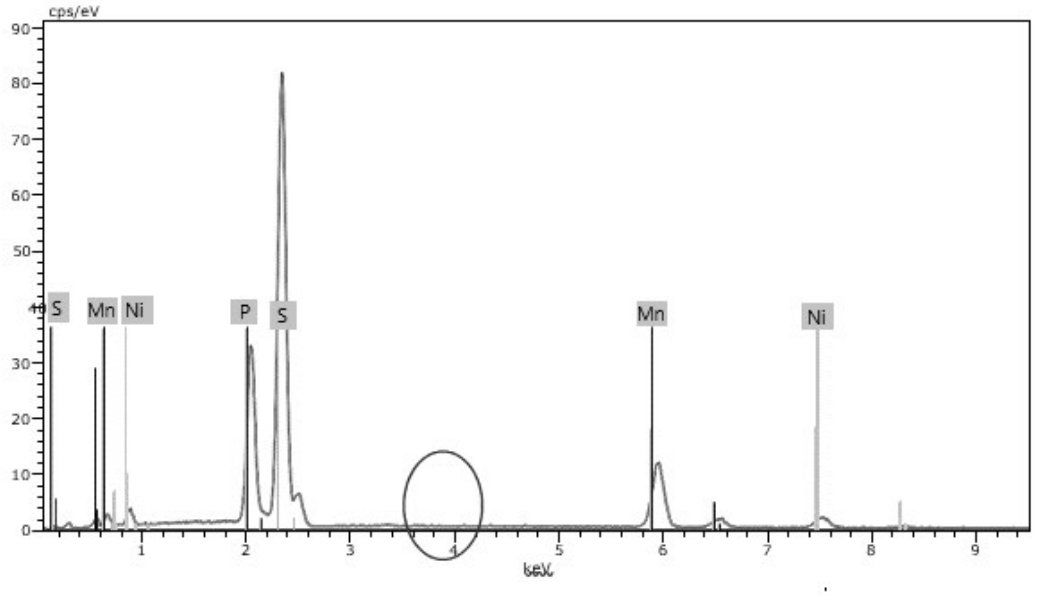

Fig S1a: EDX spectrum of bimetallic **Ni0.4** phase (circle indicates the absence of potassium ions, after the intercalation of the secondary nickel(II) ions).

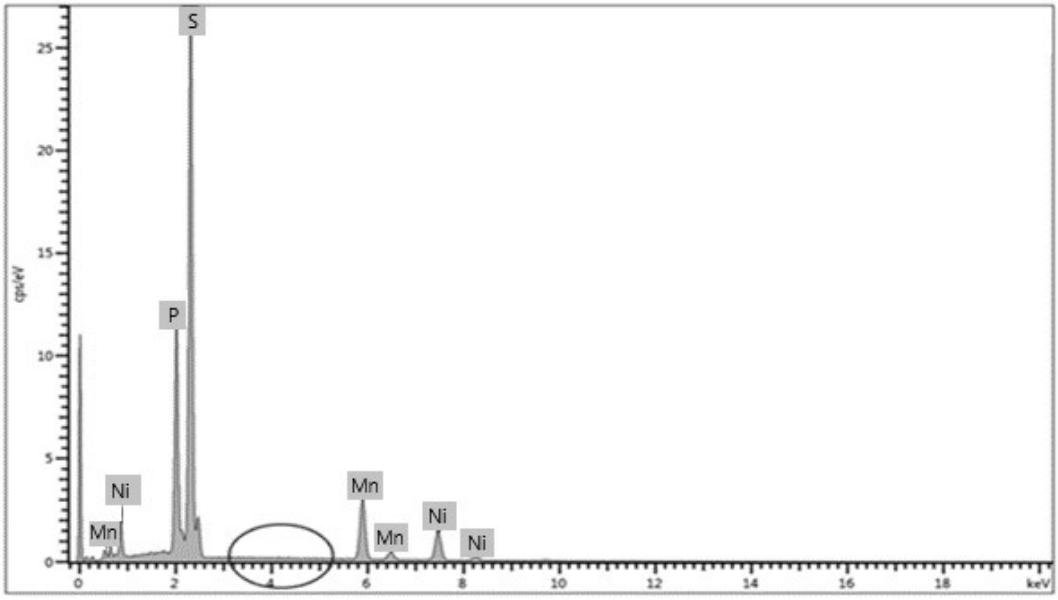

Fig S1b: EDX spectrum of bimetallic **Ni0.8** phase (circle indicates the absence of potassium ions, after the intercalation of the secondary nickel(II) ions).

.

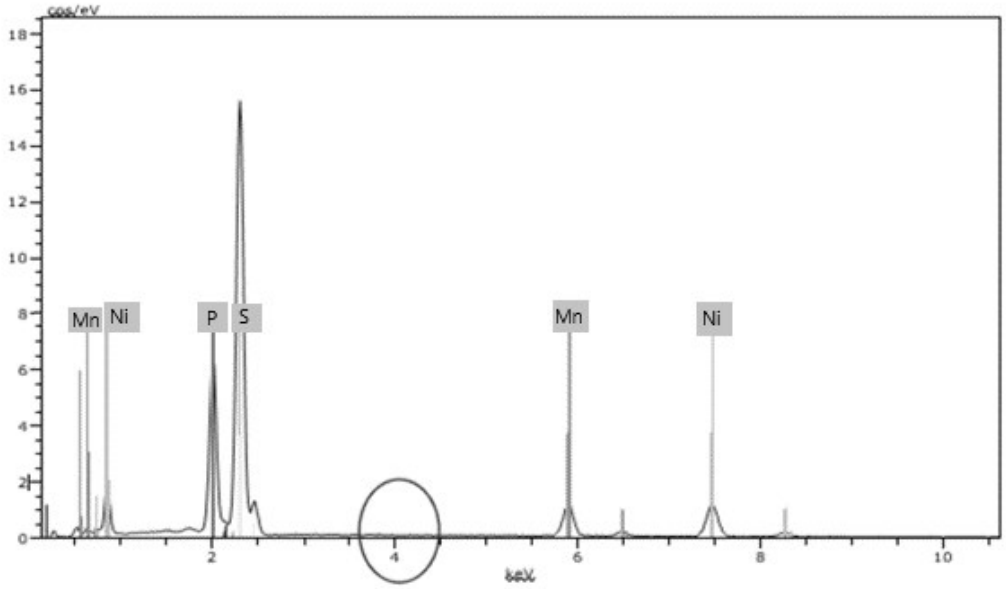

Fig S1c: EDX spectrum of bimetallic **Ni1.2** phase (circle indicates the absence of potassium ions, after the intercalation of the secondary nickel(II) ions).

.

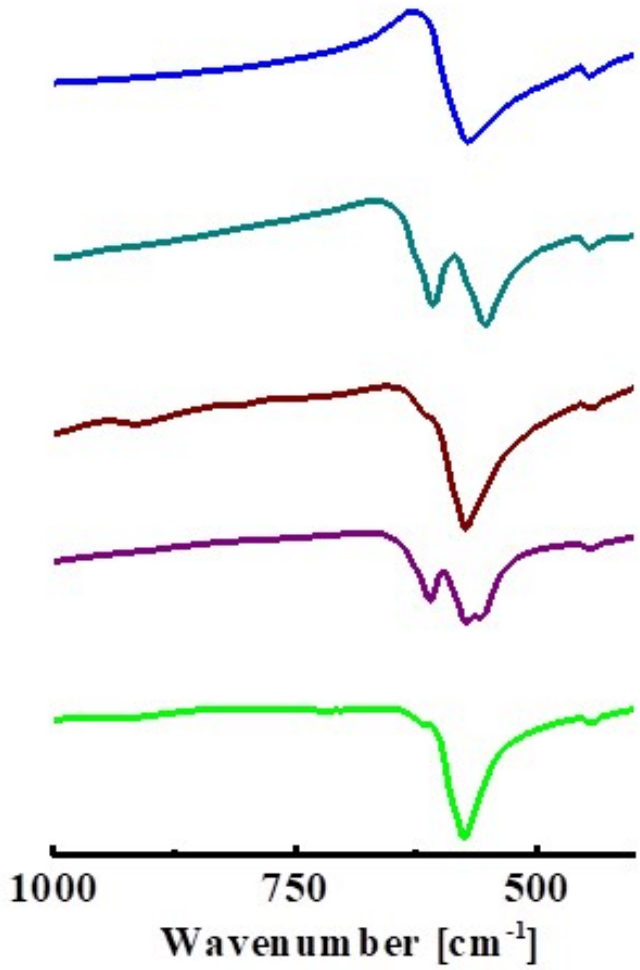

Fig.S2: Infrared spectra (FT-IR) of the bimetallic phases **Ni0.4** ♦, **Ni0.8** ♦, **Ni1.2** ♦, and the potassium intercalates $K_{0.8}Ni_{0.4}Mn_{1.2}P_2S_6 \bullet 2H_2O$ ♦; $K_{0.8}Ni_{0.8}Mn_{0.8}P_2S_6 \bullet 2H_2O$ ♦

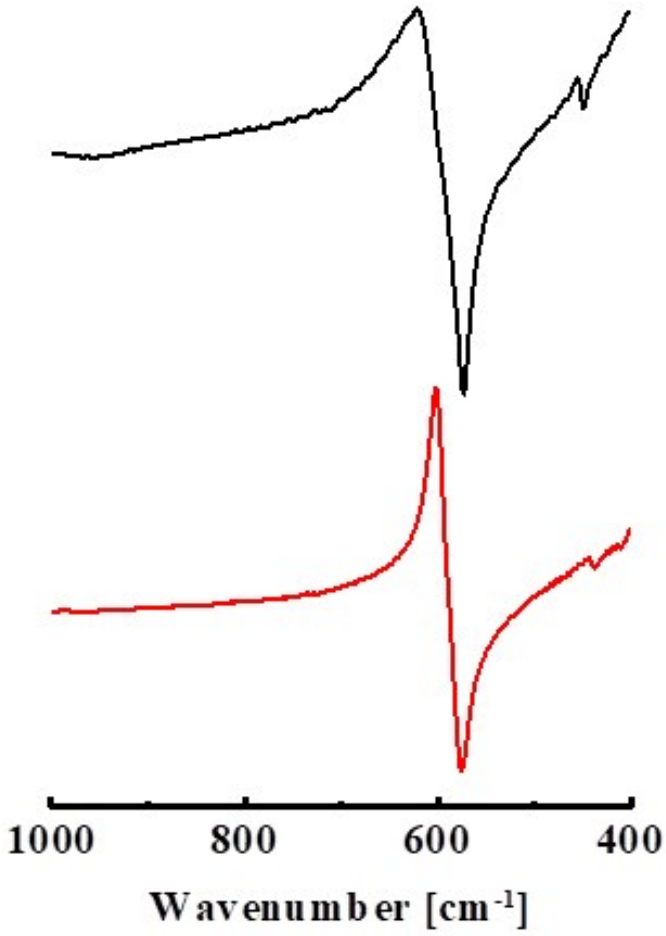

Fig. S3: Infrared spectra of pristine $Mn_2P_2S_6$ ♦ and $Ni_2P_2S_6$ ♦.

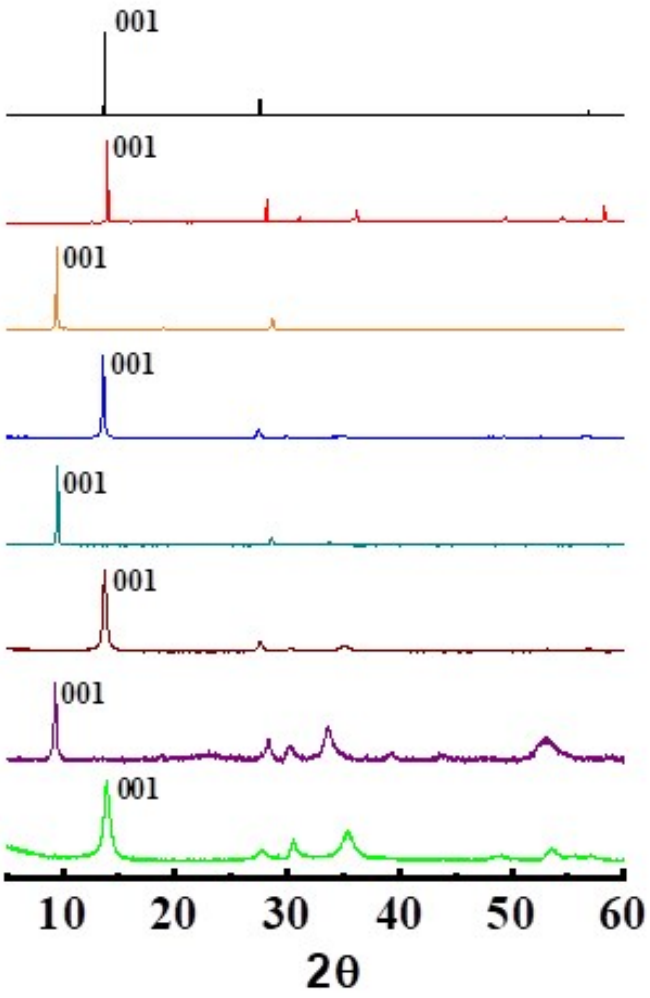

Fig.S4: Powder X-ray diffractograms of the pristine phases $Mn_2P_2S_6$ ♦, and $Ni_2P_2S_6$ ♦; $K_{0.8}Mn_{1.6}P_2S_6 \bullet 2H_2O$ ♦, $K_{0.8}Ni_{0.4}Mn_{1.2}P_2S_6 \bullet 2H_2O$ ♦ , $K_{0.8}Ni_{0.8}Mn_{0.8}P_2S_6 \bullet 2H_2O$ ♦ and bimetallic phases **Ni0.4** ♦, **Ni0.8** ♦, **Ni1.2** ♦. The interlayer distance was calculated by Bragg equation, using the value of 2θ.

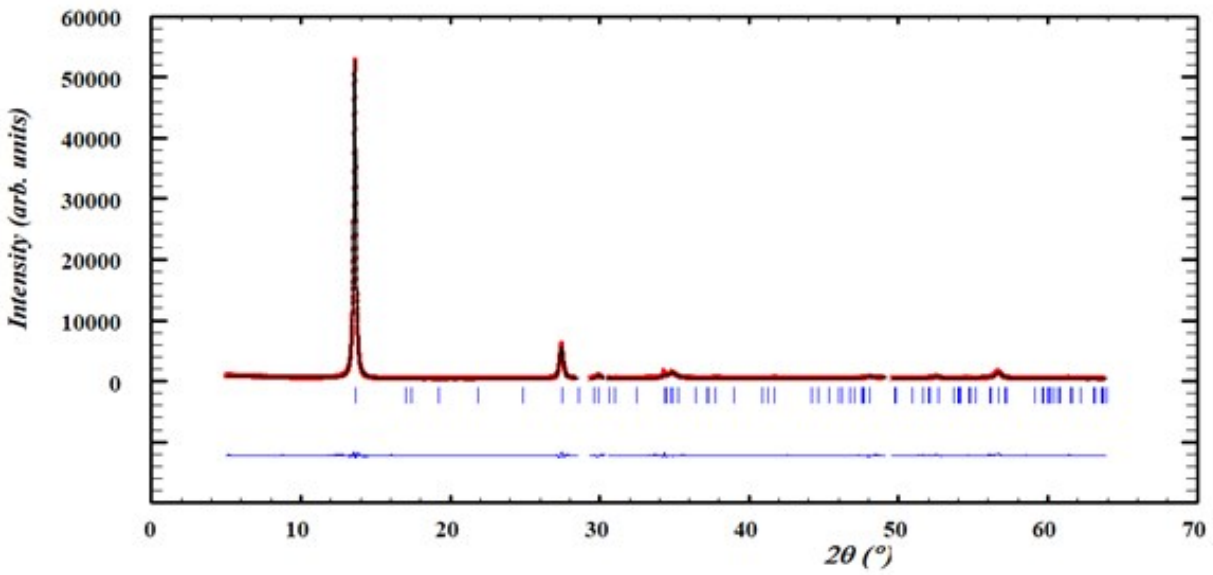

Fig.S5a: Pattern matching for **Ni0.4** bimetallic phase. The experimental pattern (red line), calculated pattern (black line), difference between experimental and calculated pattern (blue line) and Bragg positions (blue bars).

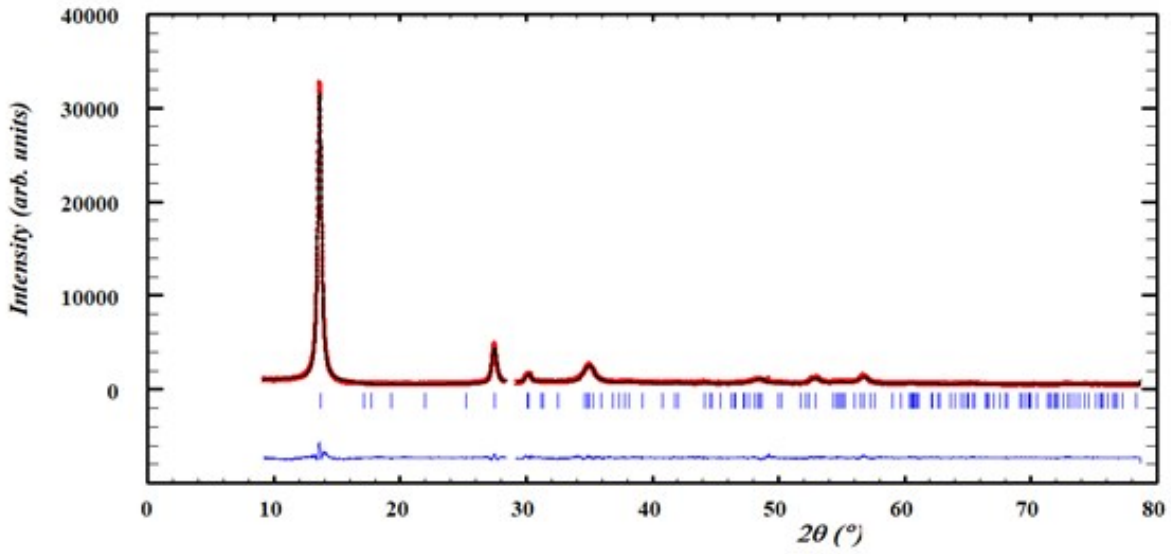

Fig.S5b: Pattern matching for **Ni0.8** bimetallic phase. The experimental pattern (red line), calculated pattern (black line), difference between experimental and calculated pattern (blue line) and Bragg positions (blue bars).

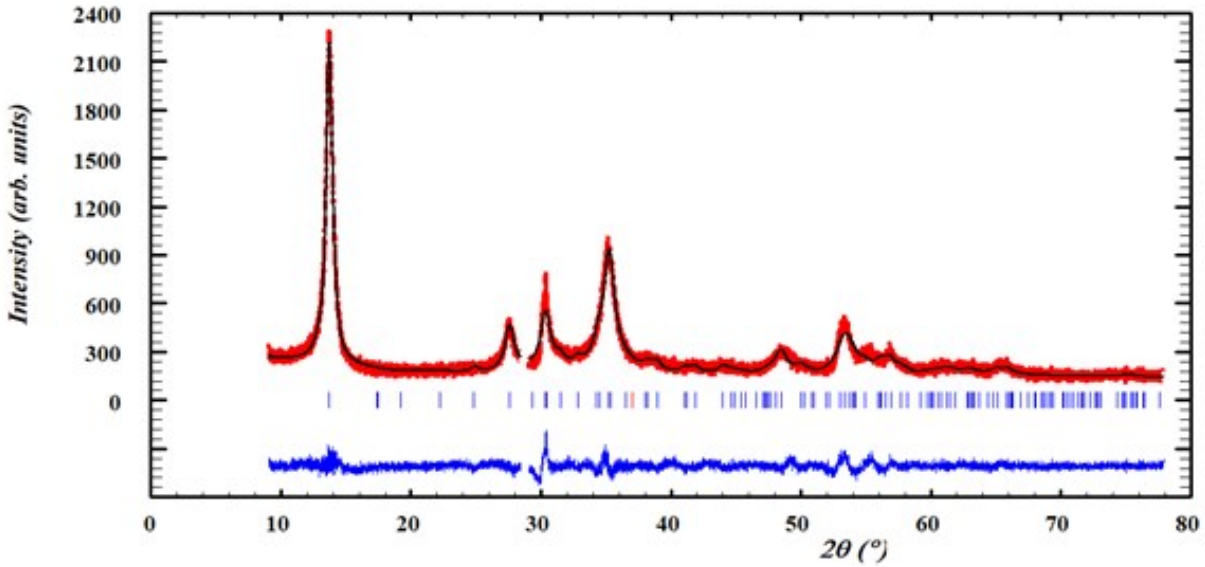

Fig.S5c: Pattern matching for **Ni1.2** bimetallic phase. The experimental pattern (red line), calculated pattern (black line), difference between experimental and calculated pattern (blue line) and Bragg positions (blue bars).

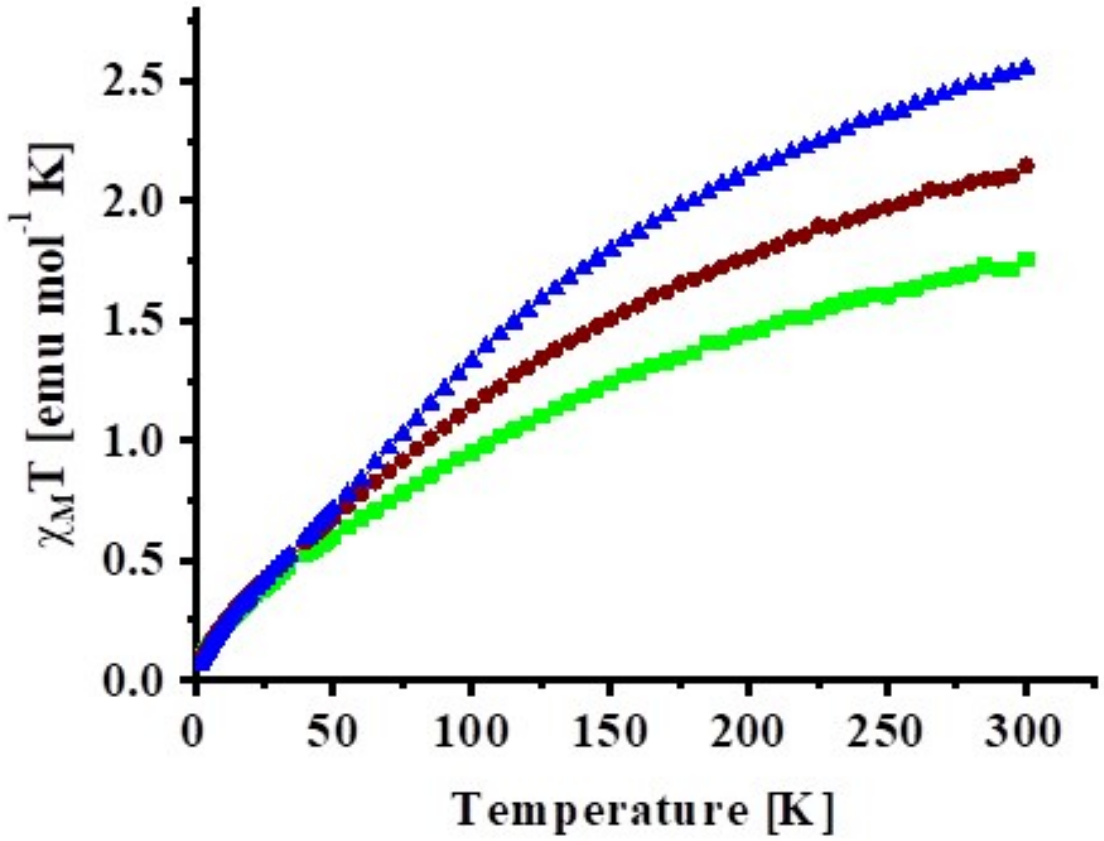

Fig.S6: $\chi_M T(T)$ curves of bimetallic phases **Ni0.4** ▲, **Ni0.8** ●, **Ni1.2** □.

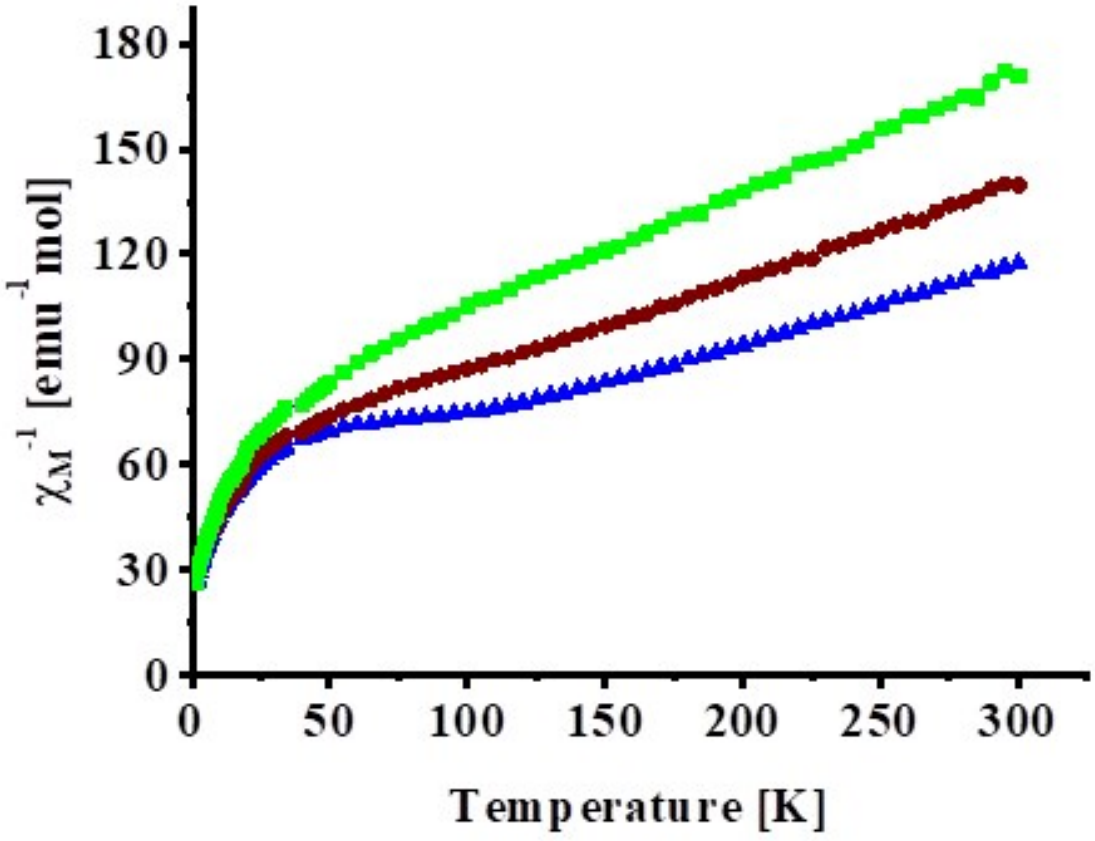

Fig.S7: χ_M^{-1}(T) curves of bimetallic phases **Ni0.4**▲, **Ni 0.8** ●, **Ni 1.2**□.

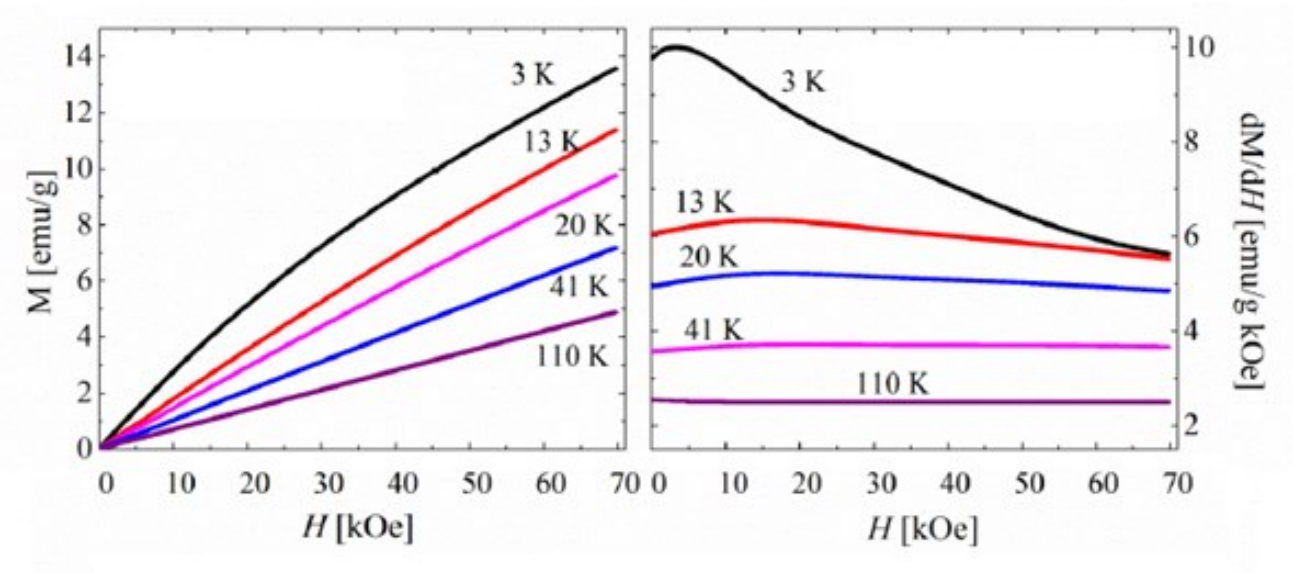

Fig. S8a: M(H) curves and first derivative dM/dH of **Ni0.4**

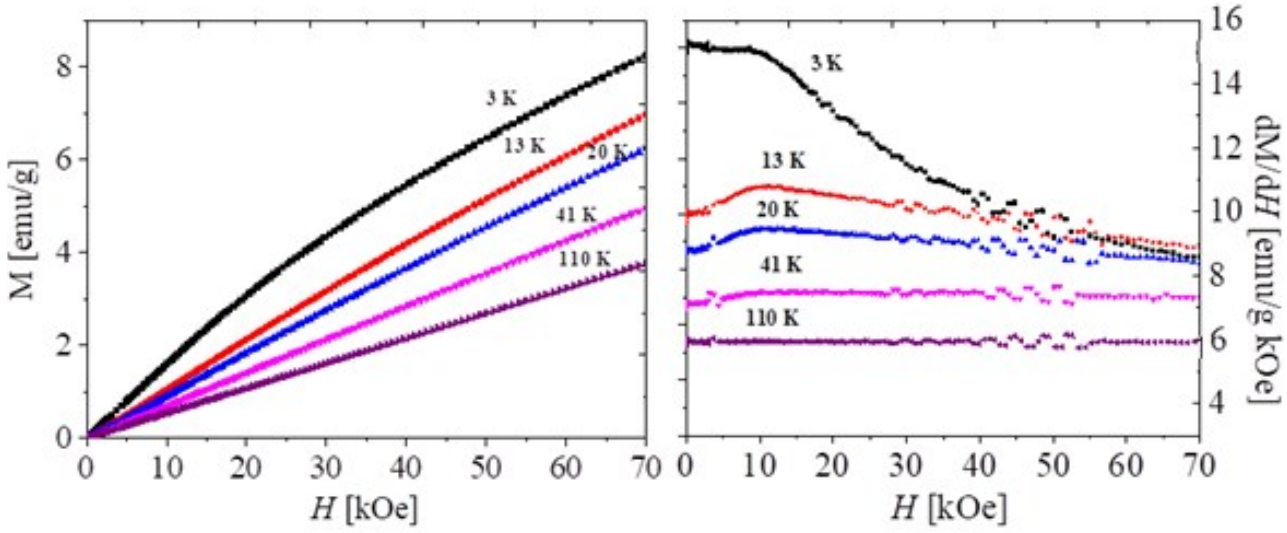

Fig. S8b: M(H) curves and first derivative dM/dH of **Ni0.8**

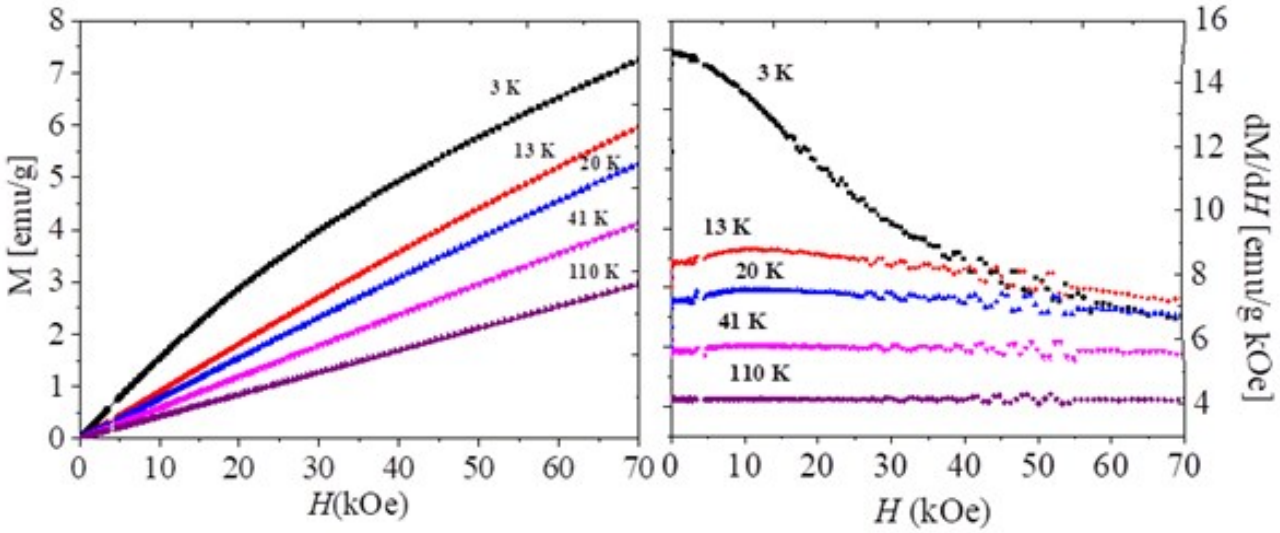

Fig. S8c: M(H) curves and first derivative dM/dH of **Ni1.2.**

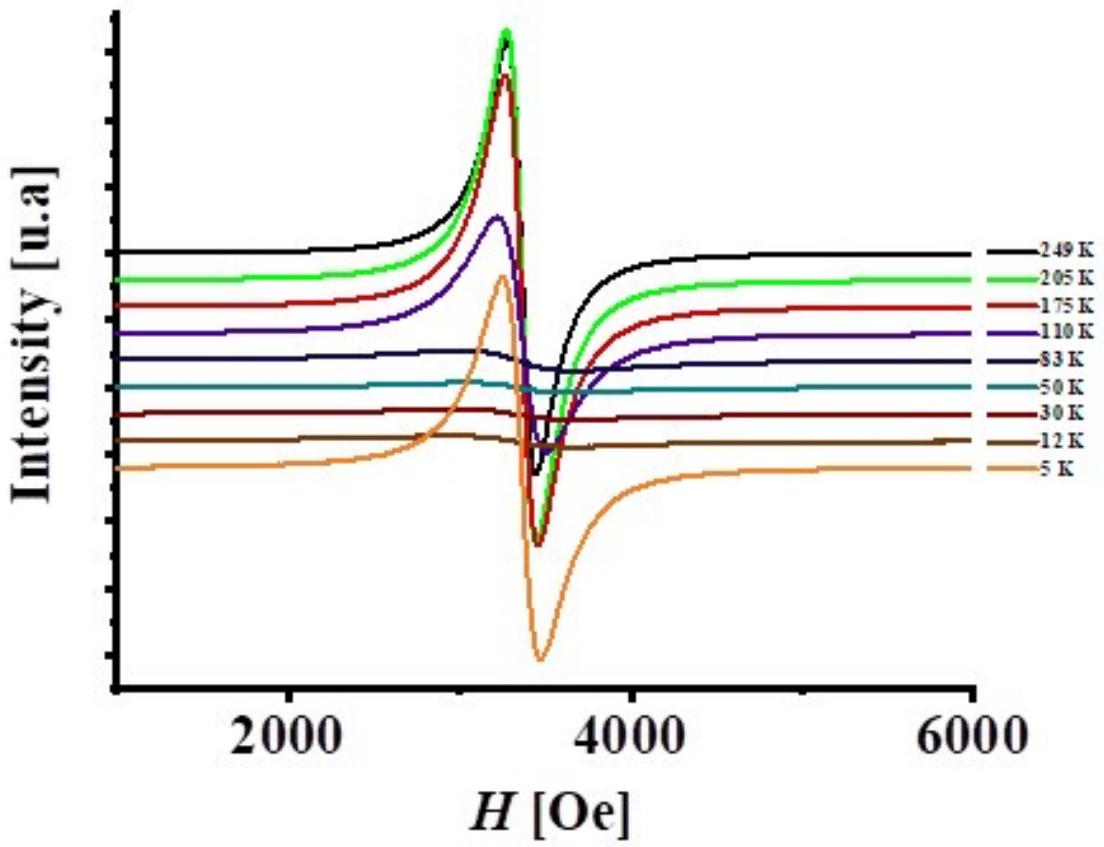

Fig.S9: EPR spectra of **Ni0.4** bimetallic phase at different temperatures.

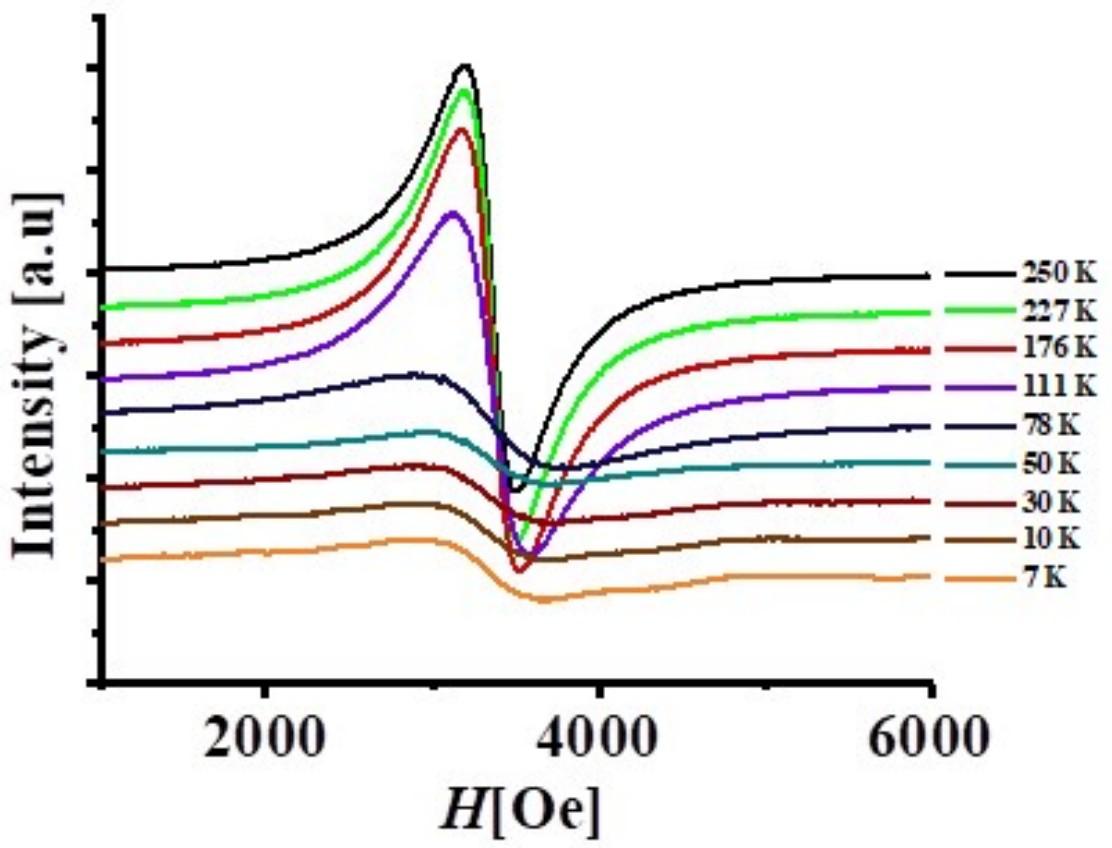

Fig.S10: Temperature dependence of EPR spectra of **Ni0.8**.

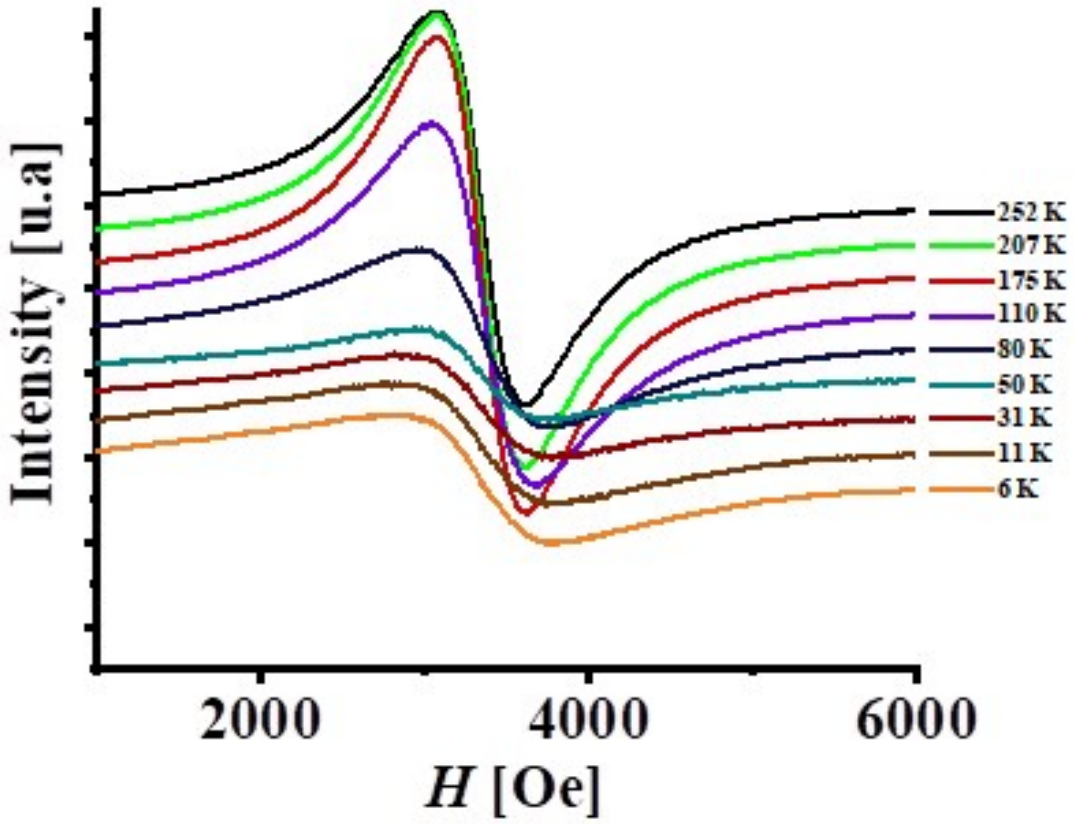

Fig.S11: EPR spectra of **Ni1.2** bimetallic phase at different temperatures.

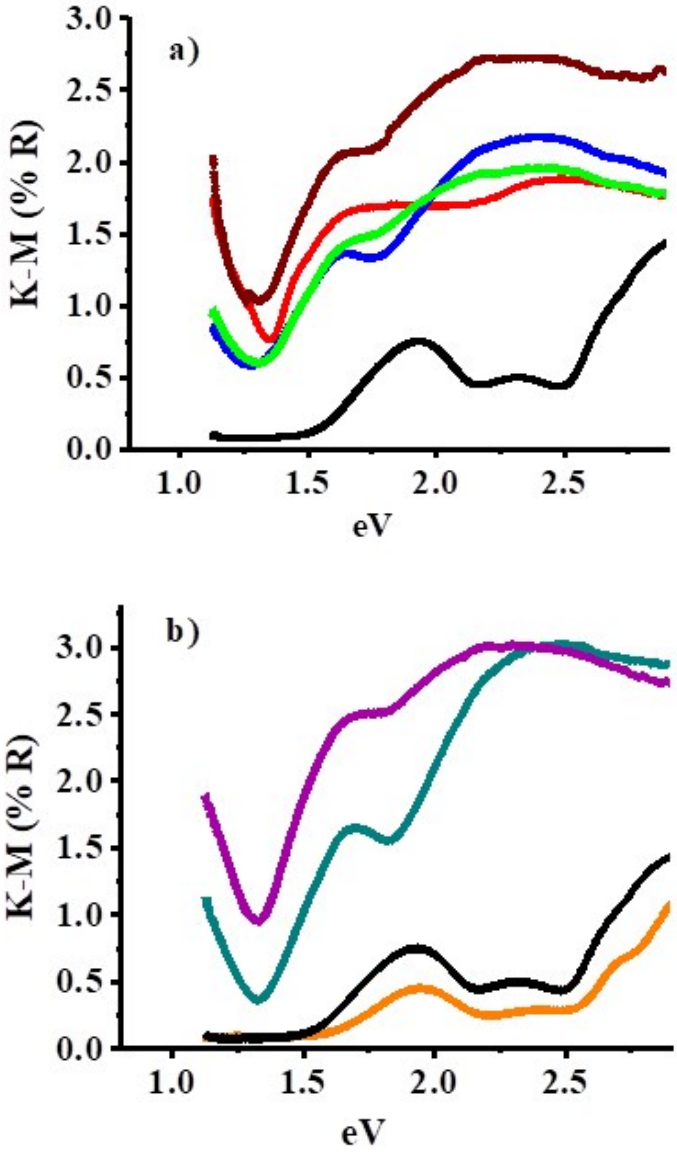

Fig.S12: **a)** Solid state UV-visible spectra of bimetallic phases **Ni0.4**, **Ni0.8**, **Ni1.2**, and the pristine phases of $Mn_2P_2S_6$, and $Ni_2P_2S_6$; **b)** Solid state UV-visible spectra of potassium precursors: $K_{0.8}Mn_{1.6}P_2S_6 \bullet 2H_2O$, $K_{0.8}Ni_{0.4}Mn_{1.2}P_2S_6 \bullet 2H_2O$, $K_{0.8}Ni_{0.8}Mn_{0.8}P_2S_6 \bullet 2H_2O$.

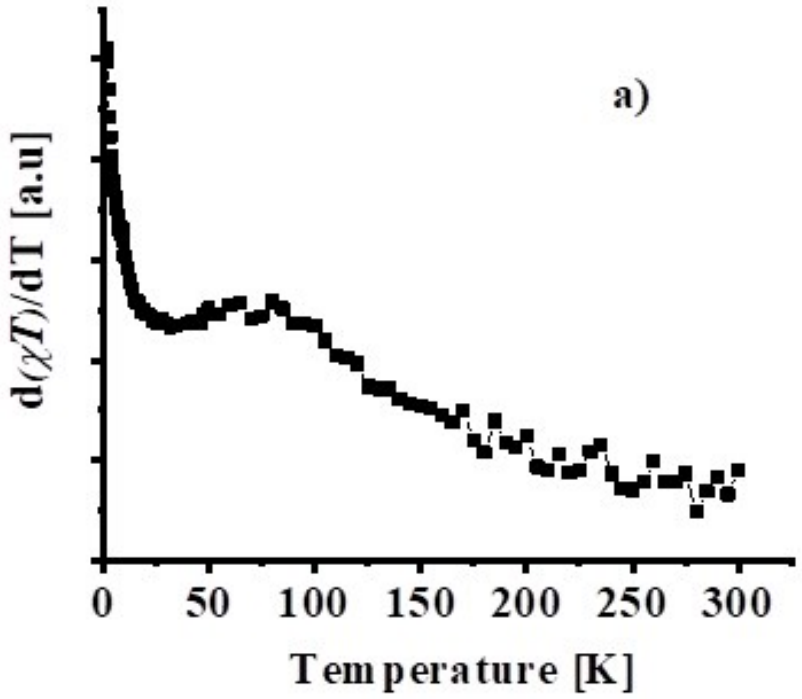
a)
d(χT)/dT [a.u]
0
50
100
150
200
250
300
Temperature [K]

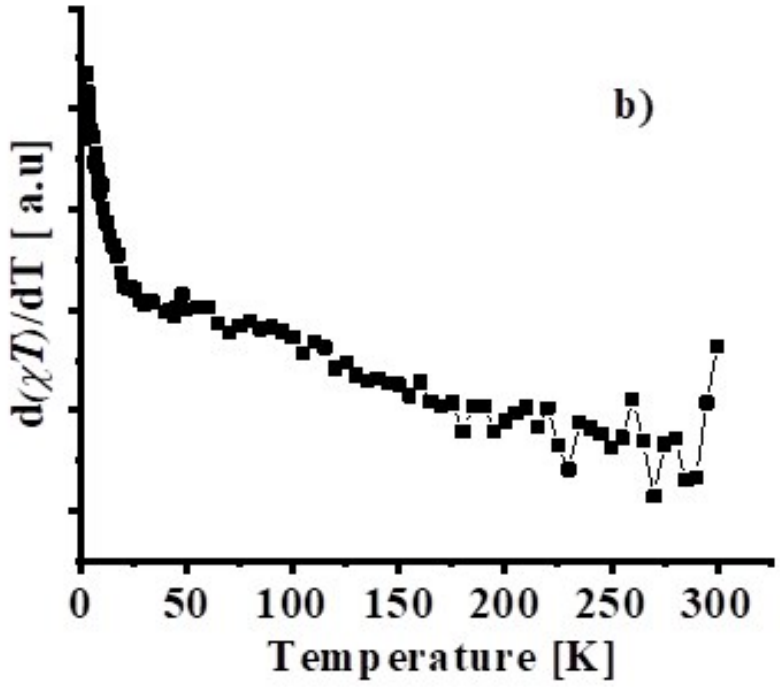
b)
d(χT)/dT [a.u]
0
50
100
150
200
250
300
Temperature [K]

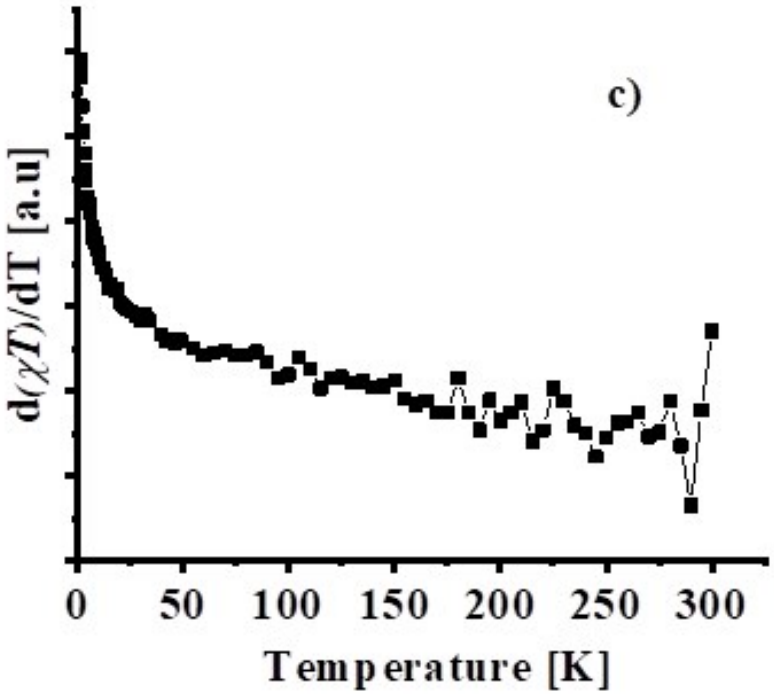

Fig.S13: First derivative of $\chi_M T(T)$ plot of bimetallic phases: a) **Ni0.4**, b) **Ni0.8** and c) **Ni1.2**

Table S1: Cell parameters and agreement factors obtained from the pattern matching of the diffractograms of bimetallic phases.

	$Mn_2P_2S_6$	Ni0.4	Ni0.8	Ni1.2	$Ni_2P_2S_6$ [1]
a	6.0819(1)	6.1030(6)	5.9859(6)	6.175(1)	5.812(2)
b	10.5268(2)	10.4129(7)	10.376(1)	10.152(3)	10.070(3)
c	6.80410(6)	6.7879(5)	6.8039(6)	6.772(1)	6.632(1)
β	107.430(1)	107.07(1)	107.715(9)	107.32(2)	106.980(3)
Chi^2	11.8	2.48	1.84	1.84	Not reported
Rp	7.15	4.11	4.52	6.41	4.7
Rwp	11.6	5.96	6.14	8.44	5.5

Table S2: 2Θ values of the 001 peak of the corresponding diffractogram, and interlayer distance of the pristine phase $Mn_2P_2S_6$, $Ni_2P_2S_6$, potassium precursors and bimetallic phases.

Phase	2θ (°)	Interlayer space (Å)
$Mn_2P_2S_6$	13.7	6.5
$Ni_2P_2S_6$	14.0	6.3
$K_{0.8}Mn_{1.6}P_2S_6 \cdot 2H_2O$	9.5	9.4
Ni0.4	13.6	6.5
$K_{0.8}Ni_{0.4}Mn_{1.2}P_2S_6 \cdot 2H_2O$	9.5	9.4
Ni0.8	13.7	6.5
$K_{0.8}Ni_{0.8}Mn_{0.8}P_2S_6 \cdot 2H_2O$	9.4	9.4
Ni1.2	13.7	6.5

References

1. G. Ouvrard, R. Brec and J. Rouxel, *Mater. Res. Bull.*, 1985, **20**, 1181–1189.